Volume 1 | Number 1 | Jan 2013 | Pages 1–100

ChemComm

Chemical Communications
www.rsc.org/chemcomm

ROYAL SOCIETY OF CHEMISTRY

This is an *Accepted Manuscript*, which has been through the Royal Society of Chemistry peer review process and has been accepted for publication.

Accepted Manuscripts are published online shortly after acceptance, before technical editing, formatting and proof reading. Using this free service, authors can make their results available to the community, in citable form, before we publish the edited article. We will replace this *Accepted Manuscript* with the edited and formatted *Advance Article* as soon as it is available.

You can find more information about *Accepted Manuscripts* in the **Information for Authors**.

Please note that technical editing may introduce minor changes to the text and/or graphics, which may alter content. The journal's standard **Terms & Conditions** and the **Ethical guidelines** still apply. In no event shall the Royal Society of Chemistry be held responsible for any errors or omissions in this *Accepted Manuscript* or any consequences arising from the use of any information it contains.

ChemComm

COMMUNICATION

Redox-active conjugated microporous polymers: a new organic platform for highly efficient energy storage

Fei Xu,[a,b] Xiong chen,[a] Zhiwei Tang,[b] Dingcai Wu,[b] Ruowen Fu,[b] and Donglin Jiang*,[a]

**Conjugated microporous polymers are developed as a new platform for lithium-battery energy storage, which features near-unity coulombic efficiency, high capacity and cycle stability. The polymers exhibit synergistic structural effects on facilitating charge dynamics by virtue of their built-in redox skeletons, open nanopores and large surface areas.**

Conjugated microporous polymers (CMPs) are a unique class of polymers that combine π-conjugated skeletons with permanent nanopores,[1,2] which are hardly available with other porous materials. The diversity of organic building blocks and the availability of various conjugated linkages endow CMPs with a high flexibility in the molecular design of both skeletons and pores. CMPs have emerged as a powerful platform for synthesizing functional polymers that exhibit outstanding functions, such as gas storage,[3,4] superabsorption,[5] light emitter,[6] light-harvesting antennae,[7] sensors,[8] and catalysts.[9,10] Different from other porous carbon materials, CMPs with designable π skeletons and nanopores are fascinating for developing energy-storage devices.[1a,11] However, the successful example has been very limited to only supercapacitors.[11a] CMPs for energy storage remain to be well explored.

Here we report the synthesis and energy storage properties of a newly designed hexaazatrinaphthalene CMP (Scheme 1, HATN-CMP) with built-in redox-active skeletons and permanent nanopores. The CMP strategy provides a useful platform for crosslinking redox-active modules into highly stable porous electrodes; such organic cathode materials have been long pursued in the exploration of next-generation green batteries.[12,13] We highlight that the structural features of the CMP work together in energy storage with lithium-ion batteries because the HATN-CMP skeleton is built from redox-

active units that serve as energy-storing and power-supplying modules, it bears inherent open nanopores that are accessible to lithium ions and it possesses high surface area that facilitates the charge dynamics. As a result, the HATN-CMP permits the utilization of Columbic charges in a near-unity efficiency, exhibits high capacity and shows outstanding cycle stability.
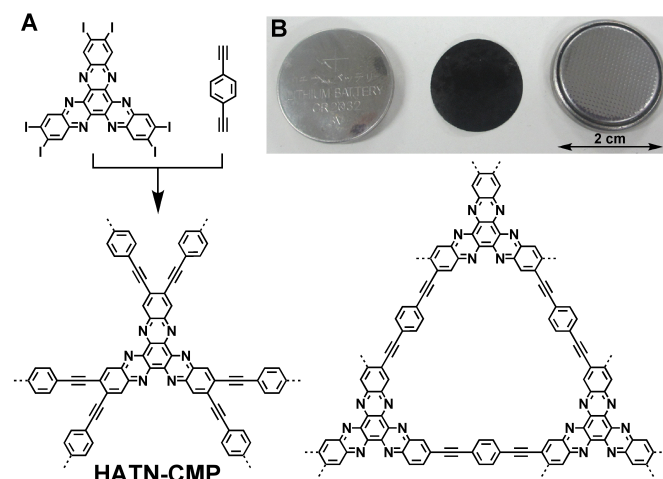
Scheme 1 (A) Schematic representation of the synthesis of hexaazatrinephthalene CMP (HATN-CMP) and the elementary pore structure. (B) The photos of HATN-CMP electrodes and lithium batteries thus fabricated.

HATN-CMP was synthesized by the Sonogashira cross-coupling polycondensation of 1,4-diethynylbenzene, and 2,3,8,9,14,15-hexaiododiquinoxalino[2,3-a:2',3'-c]phenazine in the presence of tetrakis-(triphenylphosphine) palladium and copper iodide catalyst and diisopropylamine base (ESI†). Infrared spectroscopy confirmed the nearly completeness of the cross-coupling reaction, as evidenced by the disappearance of C–I (684 cm^{-1}) and terminal alkyne C≡CH (2102 cm^{-1}) vibrations, together with the blue shift of the alkyne C≡C vibrations (2199 cm^{-1}) in HATN-CMP compared with the monomers (Fig. S1, ESI†). Field-emission scanning electron microscopy (FE-SEM) revealed that HATN-CMP was obtained as

[a]Department of Materials Molecular Science, Institute for Molecular Science, National Institutes of Natural Sciences, 5-1 Higashiyama, Myodaiji, Okazaki 444-8787, Japan; E-mail: jiang@ims.ac.jp
[b]Materials Science Institute, PCFM Laboratory, School of Chemistry and Chemical Engineering, Sun Yat-sen University, Guangzhou, 510275, P. R. China.
†Electronic Supplementary Information (ESI) available: Materials and methods, IR, XRD and TGA profiles, FE-SEM images, discharge curves, potential profiles. See DOI: 10.1039/c000000x/

nanoparticles with size of about 100 nm, which further aggregated randomly and gave rise to interconnected meso- and macroporous gel-like objects (Fig. 1A). High-resolution transmission electron microscopy (HR TEM) revealed the presence of micropores that originated from highly crosslinked 3D molecular skeletons (Fig. 1B). The porous frameworks are amorphous without showing any clear peaks in powder X-ray diffraction measurements (Fig. S2, ESI†). HATN-CMP is thermally stable without decomposition up to 300 °C (Fig. S3, ESI†); a high thermal stability is crucial for lithium batteries from the viewpoint of safety.
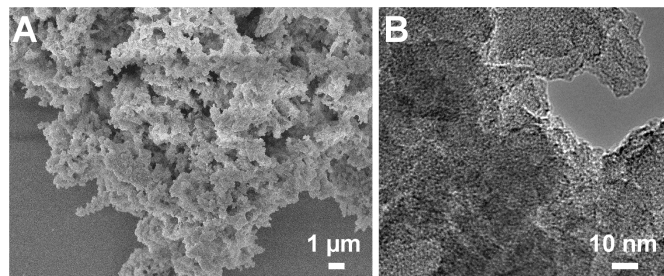

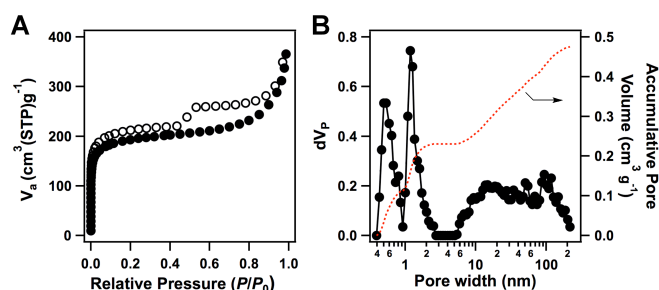Fig. 1 (A) FE-SEM and (B) HR TEM images of typical HATN-CMP samples.

Fig. 2 (A) Nitrogen sorption isotherm curves measured at 77 K (black circles: adsorption, white circles: desorption). (B) Pore-size distribution profile (black) and cumulative pore volume profile (red) calculated using the NLDFT method.

The porosity of HATN-CMP was revealed by N_2 sorption isotherm measurements at 77 K (Fig. 2A). The sorption profile exhibited an obvious uptake at low relative pressure ($P/P_0 < 0.1$), demonstrating the microporous character of the framework. One may notice that there exists a large hysteresis loop in the medium relative pressure around $P/P_0 = 0.5$, which indicates the presence of mesopores. Moreover, further increase of the relative pressure triggered a further increase in adsorption without a plateau even when the relative pressure reached 1.0; this sorption character suggests the presence of macropores between nanoparticles. The Brunauer–Emmett–Teller (BET) surface area was evaluated to be 616 m^2 g^{-1}, whereas the micropore surface area was 433 m^2 g^{-1}, accounting for 70% of the BET surface area. The total pore volume was calculated to be 0.63 cm^3 g^{-1} according to single point adsorption at $P/P_0 = 0.98$. The pore size distribution curve (Fig. 2B) based on the nonlocal density function theory (NLDFT) method revealed that the micropores are centered at 0.5 and 1.2 nm, whereas the meso- and macropores are rather broad from 6 to 200 nm that account for 30% of the BET surface area. These insights into the porosity indicate that HATN-CMP is a unique conjugated polymer that constitutes a hierarchical porous structure with micro-, meso-, and macropores. This well-developed porous architecture is highly desired for batteries because it facilitates ion transport from the

electrolyte solution to the redox-active sites within the organic frameworks.

With the above unique structural characters in mind, we fabricated the CR2032-type coin cells with HATN-CMP as cathode materials (Scheme 1B). Haxaazatrinaphthalene (HATN) is a six-electron redox-active compound.[14] The cathode was prepared by spreading the slurry of HATN-CMP, acetylene black and PVDF in NMP on aluminium foil followed by removal of NMP in high vacuum (ESI†). The FE-SEM images of the as-prepared cathode exhibited a homogenous mixing between HATN-CMP and acetylene black (Fig. S4, ESI†). Fig. 3A shows charge-discharge profile under a current density of 100 mA g^{-1}. The charge process (blue curve) exhibited a quick rise in capacity to 133 mAh g^{-1}. In the discharge process (red curve), a quick release of energy was observed at the initial stage followed by a sluggish discharge until 1.5 V. The working potential of HATN-CMP was ranged from 1.5 to 4.0 V versus Li/Li$^+$. From the discharge curve, HATN-CMP exhibited a capacity as high as 147 mAh g^{-1}. Taking account of the six-electron involved redox reaction of the HATN unit, the theoretical capacity was calculated to be 214 mAh g^{-1} (ESI†). Therefore, HATN-CMP achieves a capacity that is as high as 71% of the theoretical capacity. This result is remarkable when compared with the monomeric HATN used as a cathode, which exhibited an initial discharge capacity of 52 mAh g^{-1}, only 56% of the theoretical capacity. These results indicate that the CMP skeleton makes much efficient utilization of the redox-active units for the energy storage and power supply, because the hierarchical porous structure facilitate the access of electrolyte ions to the redox-active HATN units.
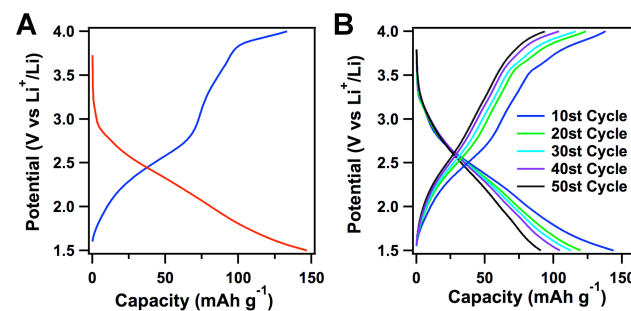

Fig. 3 (A) Charge (blue) and discharge (red) profiles of the first cycle under 100 mA g^{-1}. (B) Representative charge and discharge profiles of the HATN-CMP cells for 50 cycles.

The performance stability of HATN-CMP was tested by cycling experiments. Under a current density of 100 mA g^{-1}, HATN-CMP exhibited reversible charge-discharge curves for each cycle. Upon 50 cycles, both the charge and discharge curves retain their shapes well (Fig. 3B). After 50 cycles, HATN-CMP exhibited a capacity of 91 mAh g^{-1} (Fig. 4A) which is much higher than that of monomeric HATN (13 mAh g^{-1}). HATN-CMP exhibited a gradually decreasing tendency to reach 62% retention of the original capacity upon 50 cycles (Fig. 4B, red curve). In contrast, the monomeric HATN displayed a sharp drop in capacity to 36 mAh g^{-1} upon only 2 cycles, losing 30% of the original capacity (black curve). The monomeric HATN further decreased the capacity steadily and gave rise to only 25% retention upon 50 cycles. This significant decrease of capacity is related to the undesired leak of HATN to the electrolyte. The monomeric HATN in the cathode (for example, HATN on the electrode surface) is easily dissolved into the electrolyte, which causes a sharp decrease upon only two cycles and steady deterioration upon further cycle. In sharp contrast, the HATN units of HATN-CMP are interweaved in the network, which greatly decreases the leak of the HATN units into the electrolyte, whereas

only the HATN edges may have the possibility of leak during the repetitive charge and discharge processes. Therefore, the CMP architecture endows the batteries with not only the highly efficient utilization of active units but also the enhanced cycling performance. We calculated the coulombic efficiency by discharge/charge capacity, which reflects the efficiency of charges and ions utilized for the electrochemical reaction. To our surprise, the HATN-CMP retained a similar coulombic efficiency as high as 100% upon 50 cycles, demonstrating the high efficiency utilization of charges and ions for energy storage and supply without side reactions.
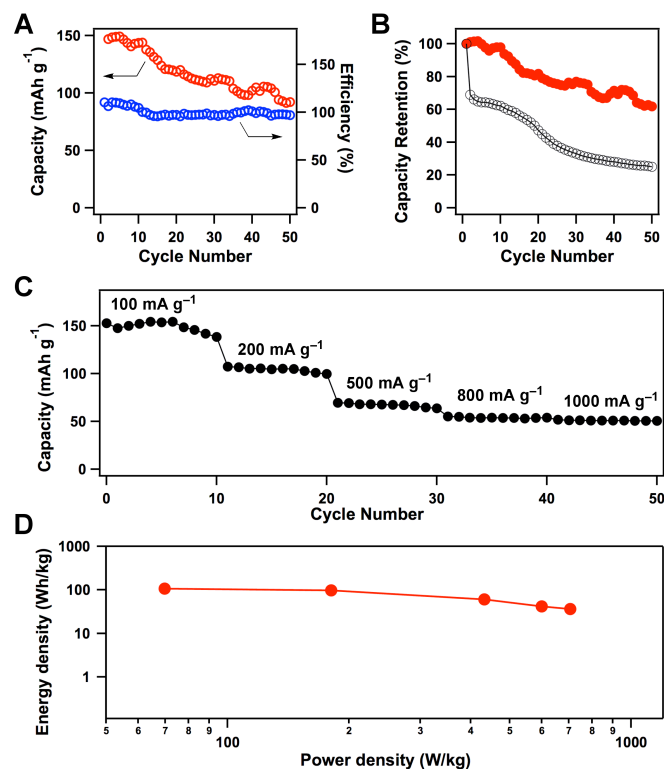
involved in the energy storage and power supply. The HATN-CMP batteries exhibit near-unity coulombic efficiency, high capacity and energy density, and enable repetitive energy storage and supply with good cycle stability. These remarkable results demonstrate the enormous potential of CMPs as green electrode materials for designing high-energy storage and power supply devices.

Fig. 4 (A) Cycle stability and (B) Capacity retention ratio of HATN-CMP (filled circle) and monomer (open circle) cathode electrodes within 50 cycle under 100 mA g^{-1}. (C) Capacity at different charge-discharge rate from 100 to 1000 mA g^{-1} with each 10 cycles, respectively. (D) Ragone plot of HATN-CMP lithium batteries.

Along this line, we investigated HATN-CMP for rapid charge and discharge cycles. The HATN-CMP battery was tested by 10 cycles for each current density increased from 100 to 200, 500, 800, and 1000 mA g^{-1}. The capacity decreased as the current density was increased (Fig. 4C, Fig. S5, ESI†). At the current density of 200 mA g^{-1}, the capacity was retained at 100 mAh g^{-1}, which decreased to 65 mAh g^{-1} when was charged and discharged at 500 mA g^{-1}. Further increment to 800 and 1000 mA g^{-1} did not cause a further loss of capacity and reached a stable value of 50 mAh g^{-1}. These results indicate that HATN-CMP enables a quick charge and discharge process and allows operations at high current density. Ragone plot revealed that the energy density was ranged between 36.5 and 106 Wh kg^{-1}, whereas the power density was 70 to 706 W kg^{-1} (Fig. 4D).

In summary, we have explored CMP architectures for energy storage and power supply with rechargeable lithium batteries, through the construction of crosslinked porous framework with built-in redox-active skeletons and high surface area nanopores. The crosslinked skeletons, the redox-active units, and the hierarchical nanopores work together and facilitate the electrochemical processes

Notes and references

1   (a) Y. Xu, S. Jin, H. Xu, A. Nagai and D. Jiang, *Chem. Soc. Rev.*, 2013, **42**, 8012; (b) A. Cooper, *Adv. Mater.*, 2009, **21**, 1291; (c) D. Wu, F. Xu, B. Sun, R. Fu, H. He and K. Matyjaszewski, *Chem. Rev.*, 2012, **112**, 3959.

2   (a) J. Jiang, F. Su, A. Trewin, C. Wood, N. Campbell, H. Niu, C. Dickinson, A. Ganin, M. Rosseinsky, Y. Khimyak and A. Cooper, *Angew. Chem. Int. Ed.*, 2007, **46**, 8574; (b) J. Jiang, F. Su, A. Trewin, C. Wood, H. Niu, J. Jones, Y. Khimyak and A. Cooper, *J. Am. Chem. Soc.*, 2008, **130**, 7710.

3   (a) R. Dawson, A. Cooper and D. Adams, *Polym. Int.*, 2013, **62**, 345; (b) R. Dawson, D. Adams and A. Cooper, *Chem. Sci.*, 2011, **2**, 1173; (c) X. Zhu, C. Tian, S. Mahurin, S. Chai, C. Wang, S. Brown, G. Veith, H. Luo, H. Liu and S. Dai, *J. Am. Chem. Soc.*, 2012, **134**, 10478; (d) Y. Xie, T. Wang, X. Liu, K. Zou and W. Deng, *Nat. Commun.*, 2013, **4**, doi: 10.1038/ncomms2960; (e) X. Liu, H. Li, Y. Zhang, B. Xu, A. Sigen, H. Xia and Y. Mu, *Polym. Chem.*, 2013, **4**, 2445; (f) A. Bhunia, V. Vasylyeva and C. Janiak, *Chem. Commun.*, 2013, **49**, 3961.

4   (a) A. Li, R. Lu, Y. Wang, X. Wang, K. Han and W. Deng, *Angew. Chem. Int. Ed.*, 2010, **49**, 3330; (b) C. Xu and N. Hedin, *J. Mater. Chem. A*, 2013, **1**, 3406.

5   (a) X. Liu, Y. Xu, Z. Guo, A. Nagai and D. Jiang, *Chem. Commun.*, 2013, 49, 3233; (b) A. Li, H. Sun, D. Tan, W. Fan, S. Wen, X. Qing, G. Li, S. Li and W. Deng, *Energ. Environ. Sci.*, 2011, **4**, 2062; (c) K. Rao, S. Mohapatra, T. Maji and S. George, *Chem. Eur. J.*, 2012, **18**, 4505; (d) X. Wang, J. Liu, J. Bonefont, D. Yuan, P. Thallapally and S. Ma, *Chem. Commun.*, 2013, **49**, 1533.

6   (a) Y. Xu, L. Chen, Z. Guo, A. Nagai and D. Jiang, *J. Am. Chem. Soc.*, 2011, **133**, 17622; (b) Y. Xu, A. Nagai and D. Jiang, *Chem. Commun.*, 2013, **49**, 1591; (c) J. Jiang, A. Trewin, D. Adams and A. Cooper, *Chem. Sci.*, 2011, **2**, 1777; (d) L. Sun, Z. Liang, J. Yu and R. Xu, *Polym. Chem.*, 2013, **4**, 1932.

7   L. Chen, Y. Honsho, S. Seki and D. Jiang, *J. Am. Chem. Soc.*, 2010, **132**, 6742.

8   (a) X. Liu, Y. Xu and D. Jiang, *J. Am. Chem. Soc.*, 2012, **134**, 8738; (b) Z. Xiang and D. Cao, *Macromol. Rapid. Comm.*, 2012, **33**, 1184; (c) J. Novotney and W. Dichtel, *Acs Macro Lett.*, 2013, **2**, 423; (d) W. Zhao, X. Zhuang, D. Wu, F. Zhang, D. Gehrig, F. Laquai and X. Feng, *J. Mater. Chem. A*, 2013, **1**, 13878; (e) K. Wu, J. Guo and C. Wang, *Chem. Commun.*, 2014, **50**, 695.

9   (a) L. Chen, Y. Yang and D. Jiang, *J. Am. Chem. Soc.*, 2010, **132**, 9138; (b) L. Chen, Y. Yang, Z. Guo and D. Jiang, *Adv. Mater.*, 2011, **23**, 3149; (c) J. Jiang, C. Wang, A. Laybourn, T. Hasell, R. Clowes, Y. Khimyak, J. Xiao, S. Higgins, D. Adams and A. Cooper, *Angew. Chem. Int. Ed.*, 2011, **50**, 1072; (d) Q. Liang, J. Liu, Y. Wei, Z. Zhao and M. MacLachlan, *Chem. Commun.*, 2013, **49**, 8928.

10 (a) N. Kang, J. Park, K. Ko, J. Chun, E. Kim, H. Shin, S. Lee, H. Kim, T. Ahn, J. Lee and S. Son, *Angew. Chem, Int. Ed.*, 2013, **52**, 6228; (b) H. Urakami, K. Zhang and F. Vilela, *Chem. Commun.*, 2013, **49**, 2353.

11 (a) Y. Kou, Y. Xu, Z. Guo, and D. Jiang, *Angew. Chem. Int. Ed.*, 2011, **50**, 8753; (b) F. Vilela, K. Zhang and M. Antonietti, *Energy Environ. Sci.*, 2012, **5**, 7819.

12 Z. Song and H. Zhou, *Energ. Environ. Sci.*, 2013, **6**, 2280.

13 M. Armand and J-M. Tarascon, *Nature* 2008, **451**, 652.

14 T. Matsunaga, T. Kubota, T. Sugimoto and M. Satoh, *Chem. Lett.*, 2011, **40**, 750.